

Field-induced tricritical phenomenon and multiple phases in DySbWei Liu,^{1,2,3} Dandan Liang,⁴ Fanying Meng,^{1,5} Jun Zhao,^{1,5} Wenka Zhu,^{1,*} Jiyu Fan,⁶ Li Pi,^{1,7} Changjin Zhang,¹ Lei Zhang^{Ⓞ,1,3,†} and Yuheng Zhang^{1,7}¹Anhui Key Laboratory of Condensed Matter Physics at Extreme Conditions, High Magnetic Field Laboratory, Chinese Academy of Sciences, Hefei 230031, China²Institutes of Physical Science and Information Technology, Anhui University, Hefei 230601, China³State Key Laboratory of Advanced Special Steel, Shanghai University, Shanghai, China⁴Anhui Polytechnic University, Wuhu 241000, China⁵University of Science and Technology of China, Hefei 230026, China⁶Department of Applied Physics, Nanjing University of Aeronautics and Astronautics, Nanjing 210016, China⁷Hefei National Laboratory for Physical Sciences at the Microscale, University of Science and Technology of China, Hefei 230026, China

(Received 28 May 2020; revised 26 October 2020; accepted 27 October 2020; published 10 November 2020)

Tricritical phenomenon appearing in multiple phases is a fundamental and attractive issue in condensed-matter physics. Monopnictide DySb, a candidate for potential magnetic topological semimetal with an antiferromagnetic ground state, has been found to possess complex and intriguing field-induced magnetic phase transitions. In this work, critical behaviors of single-crystal DySb are investigated systematically, which generate a series of critical exponents including $\beta = 0.244(2)$, $\gamma = 0.827(2)$, and $\delta = 4.425(1)$ for $H\parallel[001]$. The deduced critical exponents verified by Widom law and scaling equations are close to a tricritical mean-field model, suggesting a field-induced tricritical phenomenon in DySb. Based on the universality principle, a detailed H - T phase diagram around the phase transition is constructed for $H\parallel[001]$, in which a tricritical point is revealed at temperature and field of (7.5 K, 51.4 kOe) on intersected boundaries of antiferromagnetic, forced ferromagnetic, and paramagnetic phases. Moreover, a triple point is found at the intersection (9.2 K, 19.7 kOe) of paramagnetic and two kinds of antiferromagnetic states. Such a fascinating phase diagram is indicative of delicate competition and balance between multiple magnetic interactions in this system, and lays a solid foundation for future research in topological transition and criticality.

DOI: [10.1103/PhysRevB.102.174417](https://doi.org/10.1103/PhysRevB.102.174417)**I. INTRODUCTION**

Universality principle is a core concept in physics, which supplies an effective methodology to investigate and uncover phase transitions [1–3]. Critical behavior in the vicinity of a phase transition can be described by equations of states, which generates a series of critical exponents [4]. With these critical exponents, physical behaviors around the phase transition fulfill the universality principle [5]. Moreover, a detailed phase diagram can be constructed on the basis of the universal scaling, which reveals competition and balance among multiple phases and interactions. Particularly, tricriticality is a fundamental and attractive topic in condensed-matter physics [3]. A tricritical phenomenon is induced by coexistence of three phases under special conditions, where a tricritical point is used to describe the intersection of three critical lines [6]. Usually, a tricritical point arises at the boundary between the first-order and the second-order phase transitions [7]. As is known, a triple point is also a special point among different phases. However, a triple point is just an intersection of the

phase transitions of the same order, which is substantially different from a tricritical point [6].

Recently, rare-earth monopnictides RSb ($R = Y, Sc, Nd, Lu, La, Ho, \text{ or } Ce$) have triggered great interest due to their exotic physical properties, such as extremely large positive magnetoresistance (XMR) and possible topological nontrivial state in LaSb [8,9], orbital-flop-induced magnetoresistance anisotropy and coexisting channels of interactions in CeSb [10,11], and field-induced Fermi surface reconstruction in NdSb [12]. In particular, DySb stands out for its non-saturated XMR and is suggested to be a potential magnetic topological semimetal [13–15]. The crystal structure of DySb is of a rocksalt type at room temperature, i.e., cubic with space group $Fm\bar{3}m$. As temperature decreases, DySb undergoes a magnetic transition from a paramagnetic (PM) phase to an antiferromagnetic (AFM) ground state at a Néel temperature $T_N \sim 10$ K [16]. Simultaneously, the crystal structure evolves into a tetragonal one with $I4/mmm$, accompanied by a shrinkage of the c axis ($c/a = 0.993$) [16]. In the AFM ground state, magnetic moments of Dy^{3+} ions are aligned ferromagnetically in (011) planes while alternatively stacked along the [011] direction (NiO-type AFM). The magnetic ground state can be modulated by an external magnetic field to generate field-induced phase transitions. Interestingly, the transition route of magnetic states will be different if the

*Corresponding author: wkzhu@hmfl.ac.cn†Corresponding author: zhanglei@hmfl.ac.cn

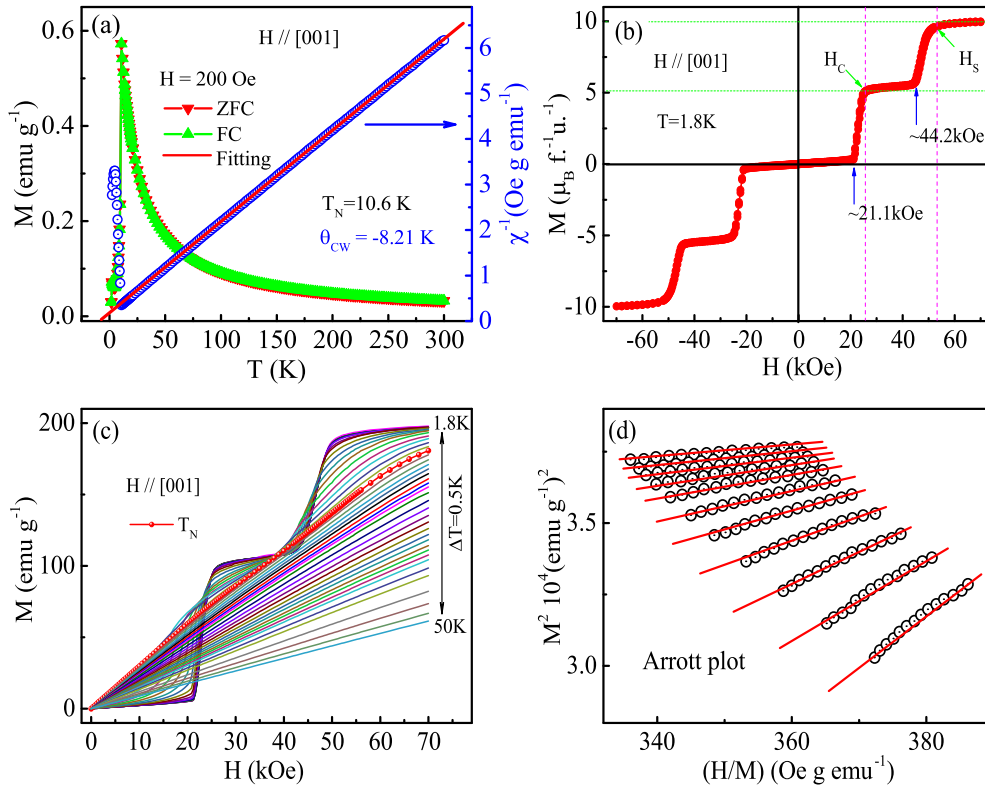


FIG. 1. (a) Temperature dependence of magnetization [$M(T)$] and reciprocal susceptibility [$\chi^{-1}(T)$] for DySb with $H \parallel [001]$; (b) isothermal magnetization [$M(H)$] at $T = 1.8$ K for $H \parallel [001]$; (c) initial isothermal $M(H)$ around phase transition temperature for $H \parallel [001]$; (d) Arrott plot in the high-field region.

external field is applied along different crystal orientations. As the field is applied along the [111] or [011] direction ($H \parallel [111]$ or $H \parallel [011]$), the AFM order is directly changed into ferromagnetic (FM) state. However, when $H \parallel [001]$, an intermediate magnetic order appears, in which the moments in one of each two nearest (011) planes are rotated by 90° to the [110] direction (HoP-type AFM). Moreover, a tricritical phenomenon has been discovered when $H \parallel [110]$, which indicates complex phases in this system [17]. Compared with $H \parallel [110]$, due to the emerged intermediate magnetic ordering for $H \parallel [001]$, more complex behaviors and magnetic interactions are expected in this direction [17].

In view of the complex phase transitions and interactions in DySb, a detailed phase diagram is desired. In this work, the critical behaviors of DySb have been investigated systematically, which reveals a field-induced tricritical phenomenon. Based on the universality principle, we construct a detailed H - T phase diagram around the phase transition for $H \parallel [001]$, in which a field-induced tricritical point and a triple point are revealed.

II. EXPERIMENTAL METHODS

Single crystals of DySb were prepared by a tin flux technique, and its physical properties were carefully checked elsewhere [13,18]. The [001] direction of the single crystal is determined by an x-ray diffraction (XRD) method [18]. The magnetization measurements, including the temperature- and field-dependent magnetization, were performed on a Quantum

Design vibrating sample magnetometer (SQUID-VSM). In particular, the initial isothermal magnetizations with $H \parallel [001]$ were carried out in detail. Before each measurement, the temperature was set at room temperature. After being held for 2 min, the sample was cooled to the target temperature. The magnetic field was quenched in an oscillation mode in order to exclude the influence of a possible remaining field. In addition, a no-overshoot mode was applied to ensure the precision of magnetic field.

III. RESULTS AND DISCUSSION

Figure 1(a) depicts the temperature dependence of magnetization [$M(T)$] and reciprocal susceptibility [$\chi^{-1}(T) = H/M$] for single-crystal DySb under a magnetic field $H = 200$ Oe. The $M(T)$ curves [left axis in Fig. 1(a)] are performed under zero-field-cooling (ZFC) and field-cooling (FC) sequences with $H \parallel [001]$. As temperature decreases, a sharp peak corresponding to the PM-AFM phase transition appears at $T_N = 10.6$ K. The ZFC and FC curves coincide with each other exactly, which is a characteristic of an AFM ground state. The $\chi^{-1}(T)$ [right axis in Fig. 1(a)] exhibits a linear behavior above T_N fulfilling the Curie-Weiss law [$\chi = C/(T - \theta_{CW})$], where C is Curie constant and θ_{CW} is Curie-Weiss temperature. Fitting to the Curie-Weiss law gives $\theta_{CW} = -8.21$ K. Such a negative value is usually connected to an AFM coupling. Figure 1(b) shows the field-dependent magnetization [$M(H)$] at 1.8 K with $H \parallel [001]$, while those with $H \parallel [011]$ and $H \parallel [111]$ are given in the Supplemental

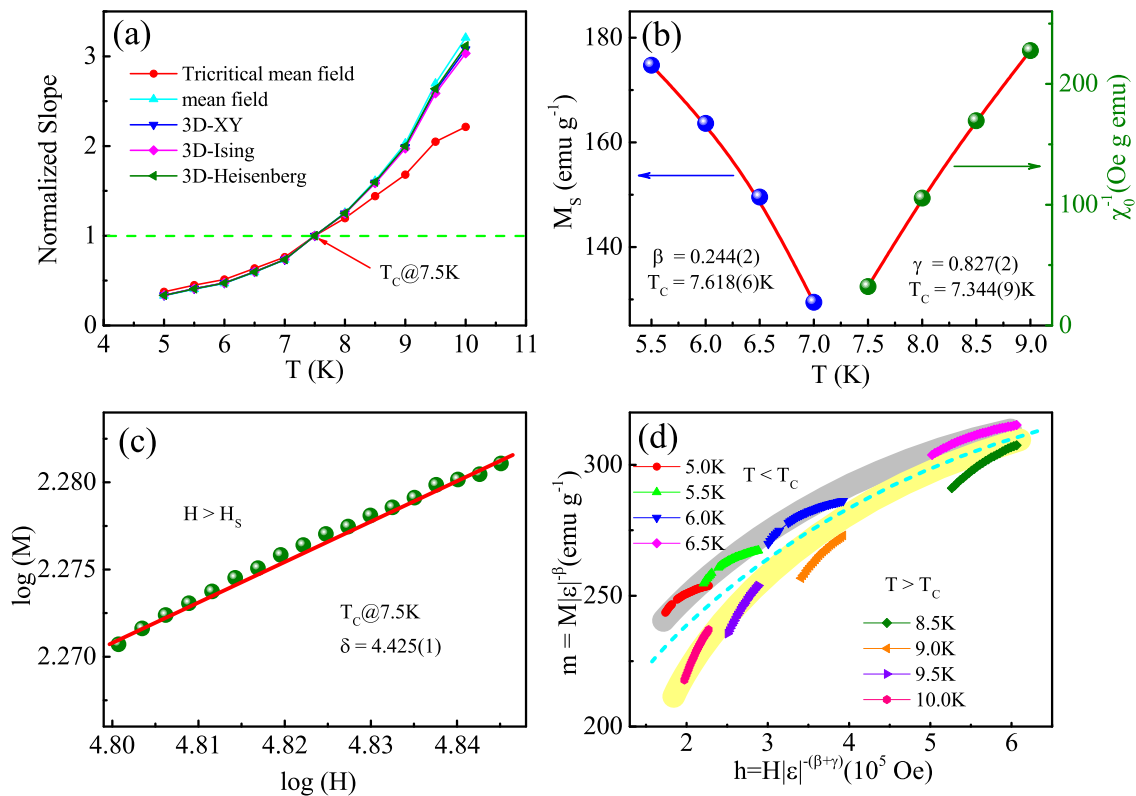


FIG. 2. (a) Normalized slopes based on different theoretical models; (b) temperature dependence of spontaneous magnetization [$M_S(T)$] and reciprocal initial susceptibility [$\chi_0^{-1}(T)$] (red curves are fitted); (c) initial isothermal $M(H)$ at the critical temperature T_c on log-log scale (red line is fitted); (d) scaling plot of the normalization magnetization m vs normalization field h around T_c in the high-field region.

Material [18]. As the field sweeps from 0 to 7 T, the $M(H)$ curve exhibits two steps, which are located at ~ 21.1 and ~ 44.2 kOe, respectively. The magnetization (M) increases very slowly below the first step at 21.1 kOe. After that it jumps to the first plateau of $\sim 5\mu_B$ /(f.u.), about half of the saturation magnetization $M_{\text{sat}} \sim 10\mu_B$ /(f.u.). Upon further increasing the field, M leaps to the second plateau, i.e., M_{sat} , corresponding to the forced ferromagnetic (FFM) phase. The two steps on the $M(H)$ curve represent two field-induced magnetic transitions. These observations are in agreement with previous reports [15,19].

In order to study the field-induced magnetic transition, initial isothermal $M(H)$ curves for $H \parallel [001]$ are measured, as shown in Fig. 1(c). For $T < T_N$, all initial $M(H)$ curves exhibit the aforementioned plateaus that shrink gradually as temperature increases. For $T > T_N$, the two steplike structures are totally suppressed and become linear ones. The initial isothermal $M(H)$ curves are in agreement with the previous report, in which the magnetic entropy change was investigated [20]. The consistency of $M(H)$ curves with other reports confirms the reliability of sample quality and experimental results. We noticed that the $M(H)$ curve exhibits a saturation behavior to the FFM state in a higher field region, which motivates us to investigate the critical behaviors on boundaries of various phases. Generally, the phase transition can be roughly judged by the Arrott plot based on the mean-field model, which is supposed to be a series of straight lines parallel to each other in the high-field region. Figure 1(d) presents the Arrott plot of M^2 vs H/M for $H \parallel [001]$, which displays a

bunch of quasistraight lines in the high-field region. However, these lines are not parallel to each other very well, implying that the mean-field model is not satisfied for DySb.

More generally, $M(H)$ curves in the vicinity of phase transition can be described by the Arrott-Noakes equation of state [21]:

$$(H/M)^{1/\gamma} = (T - T_c)/T_c + (M/M_1)^{1/\beta}, \quad (1)$$

where M_1 is a constant, and γ and β are critical exponents. The $M^{1/\beta}$ vs $(H/M)^{1/\gamma}$, called the modified Arrott plot (MAP), should consist of a bunch of parallel straight lines. In order to obtain the most appropriate critical exponents, several theoretical models are employed. As is known, the crystal structure of DySb is cubic above T_N and tetragonal below T_N [16]. Based on the three-dimensional (3D) structural characteristic, the spatial dimensionality (d) is regarded as $d = 3$. Therefore, theoretical models under the framework of $d = 3$ are preferred. The MAPs based on 3D-Heisenberg ($\beta = 0.365$, $\gamma = 1.386$), 3D-Ising ($\beta = 0.325$, $\gamma = 1.240$), 3D-XY ($\beta = 0.345$, $\gamma = 1.316$), and tricritical mean-field ($\beta = 0.25$, $\gamma = 1.0$) models are considered [22,23]. Detailed information can be found in Fig. S3 in the Supplemental Material [18]. In general, the model with the normalized slopes of $M^{1/\beta}$ vs $(H/M)^{1/\gamma}$ that are closest to “1” is the best solution to describe the critical behavior [24]. As shown in Fig. 2(a), one can see that the normalized slope based on the tricritical mean-field model is the one which deviates less from “1” among the considered models, which suggests that the tricritical mean-field

TABLE I. Comparison of critical exponents of DySb for $H\parallel[001]$ with different theoretical models (MAP = modified Arrott plot).

Composition	Technique	Ref.	T_C (K)	β	γ	δ
DySb	MAP	This work	7.5	0.244(2)	0.827(2)	4.425(1)
Tricritical mean field	Theory	[22]		0.25	1.0	5.0
3D Heisenberg	Theory	[23]		0.365	1.386	4.8
3D Ising	Theory	[23]		0.325	1.24	4.82
3D XY	Theory	[23]		0.345	1.316	4.81
Mean field	Theory	[23]		0.5	1.0	3.0

model can reflect the magnetic nature in DySb more suitably compared with other models.

Actually, in the vicinity of the magnetic phase transition, critical exponents are determined by an array of functions [4,5]:

$$M_S(T) = M_0(-\varepsilon)^\beta, \quad \varepsilon < 0, \quad T < T_C, \quad (2)$$

$$\chi_0^{-1}(T) = (h_0/M_0)\varepsilon^\gamma, \quad \varepsilon > 0, \quad T > T_C, \quad (3)$$

$$M = DH^{1/\delta}, \quad \varepsilon = 0, \quad T = T_C, \quad (4)$$

where M_S is the spontaneous magnetization, χ_0 is initial susceptibility, and M_0/h_0 and D are critical amplitudes. ε is the reduced temperature defined as $\varepsilon = (T - T_C)/T_C$, where T_C is the critical temperature denoting the field-induced phase transition temperature. The critical exponent β is associated with M_S , γ is responding to χ_0 , and δ is correlated with T_C . Precise critical exponents can be extracted by an iteration method [24]. Figure 2(b) shows the temperature dependence of spontaneous magnetization [$M_S(T)$] and reciprocal initial susceptibility [$\chi_0^{-1}(T)$]. By fitting to Eqs. (2) and (3), it is obtained that $\beta = 0.244(2)$ with $T_C = 7.618(6)$ and $\gamma = 0.827(2)$ with $T_C = 7.344(9)$. Meanwhile, the critical exponent δ can be obtained from the initial $M(H)$ taken at T_C . From Eq. (4), there is a relation of $\log(M) = \log(D) + 1/\delta \log(H)$ in the high-field region ($H > H_S$, i.e., the saturation field). Thus, $1/\delta$ can be acquired by plotting the slope of $\log(M)$ vs $\log(H)$. As shown in Fig. 2(c), $\delta = 4.425(1)$ is obtained from the linear fitting of initial $M(H)$ taken at $T_C = 7.5$ K above H_S .

The independently obtained critical exponents are unified by the Widom scaling law, which manifests their self-consistency. Therefore, the obtained critical exponents can be examined by the Widom scaling law [25,26]:

$$\delta = 1 + \frac{\gamma}{\beta}. \quad (5)$$

According to this law, δ is calculated out to be 4.387(4), very close to the experimentally obtained value. This demonstrates that the obtained critical exponents here are self-consistent, which confirms the reliability of these critical exponents. Furthermore, these critical exponents can be testified by the scaling hypothesis. Taking account of the critical exponents, $M(H)$ curves are expected to follow the scaling equations. By defining the renormalized magnetization (m) as $m \equiv \varepsilon^{-\beta} M(H, \varepsilon)$ and the renormalized field (h) as $h \equiv H \varepsilon^{-(\beta+\gamma)}$, the scaling equation in the asymptotic critical region is ex-

pressed as [5]

$$m = f_{\pm}(h), \quad (6)$$

where f_{\pm} are regular functions denoted as f_+ for $T > T_C$ and f_- for $T < T_C$. According to the universality scaling law, m vs h curves should form two independent universal branches for $T > T_C$ and $T < T_C$, respectively. With these obtained critical exponents, the initial isothermal $M(H)$ curves in the high-field region ($H > H_S$) around T_C are rescaled into $m(h)$ curves, which are depicted in Fig. 2(d). In the high-field region, $m(h)$ curves collapse onto two independent branches above and below T_C , respectively, which fulfill the universality principle.

The obtained critical exponents of DySb for $H\parallel[001]$ and theoretical models are listed in Table I for comparison. The obtained critical exponents for DySb with $H\parallel[001]$ [$\beta = 0.244(2)$, $\gamma = 0.827(2)$, $\delta = 4.425(1)$] are close to the theoretical prediction of a tricritical mean-field model ($\beta = 0.25$, $\gamma = 1.0$, and $\delta = 5.0$) except slight deviation [18,22]. The critical behavior of DySb belongs to the universality class of tricritical mean field, where the slight deviation may be due to some unexpected magnetic interactions. A tricritical phenomenon usually appears in a system hosting multiple phases. In such a system, magnetic phase can be tuned by different means such as pressure, field, fluctuation, or doping. For example, in MnSi, both field and pressure can induce a tricritical phenomenon [27,28]. In EuPtSi, which belongs to the mean-field universality class, field, or fluctuation yields a first-order transition and a tricritical point [29,30]. In double-perovskite $\text{La}_2\text{ZnIrO}_6$, the field causes a first-order AFM-FM transition and a tricritical behavior [31]. An analogous phenomenon is also observed in USb_2 , where high magnetic field destroys the AFM state to generate a tricritical behavior [32]. Recently, multiple phases with a tricritical point and a Lifshitz point are found in Cu_2OSeO_3 hosting skyrmion [33].

Figures 3(a) and 3(b) display MAPs of $M^{1/\beta}$ vs $(H/M)^{1/\gamma}$ based on the obtained critical exponents for DySb in the high-field (HF) and the low-field (LF) regions, respectively. The $M^{1/\beta}$ vs $(H/M)^{1/\gamma}$ in Fig. 3(a) in the high-field region presents a series of quasistraight lines, confirming the reliability of these critical exponents. However, the magnified MAP of $M^{1/\beta}$ vs $(H/M)^{1/\gamma}$ in the low-field region exhibits more complex behaviors. Figure 3(b) shows the magnified MAP on log-log scale in the low-field (LF) region, the inset of which gives the whole scaling region. Several turning points can be found in the MAP in Fig. 3(b), which are indications of field-induced phase transitions. The change of magnetic interactions caused by the phase transition will make the scaling curves become divergent on the phase boundary, which causes the appearance of a turning point on MAP [28,31,34]. Various

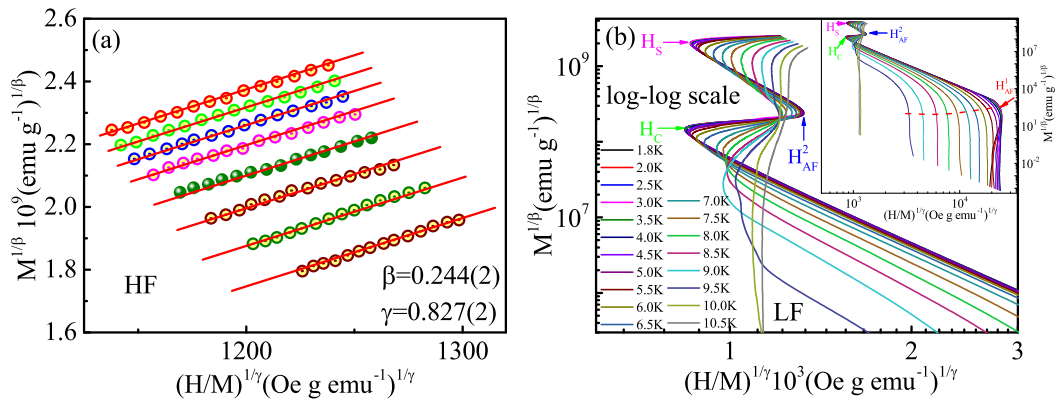


FIG. 3. (a) Modified Arrott plot (MAP) on linear scale in the high-field (HF) region; (b) magnified MAP on log-log scale in the low-field (LF) region (the inset gives the whole scaling region).

phases are separated by these turning points, based on which a detailed H - T phase diagram can be established. The boundary between PM and FM phases (T_C) is distinguished by the minimum point on the derivative $M(T)$ curve, which is shown in the Supplemental Material in detail [18]. The boundary between the AFM and FM (T_N) is determined by the peak on the $M(T)$ curve. The boundaries between the NiO-type AFM and the HoP-type one are determined by turning points in the lower-field region on MAP, which are marked as H_{AF}^1 in Fig. 3(b). Similarly, the boundaries between the HoP type and FFM are distinguished by turning points marked as H_{AF}^2 in Fig. 3(b). The coexistence regions, i.e., the phase transition region, are defined by the regions with negative slopes on MAP, because the change of slopes induced by the phase transition results in the negative slopes.

Figure 4 shows the H - T phase diagram for single-crystal DySb with $H \parallel [001]$. As is known, DySb possesses a NiO-type AFM ground state at low temperature [35], which is illustrated in the lower inset of Fig. 4. Upon increasing the field, the NiO-type AFM evolves into a HoP-type AFM gradually. From the phase diagram in Fig. 4, one can see that these two types

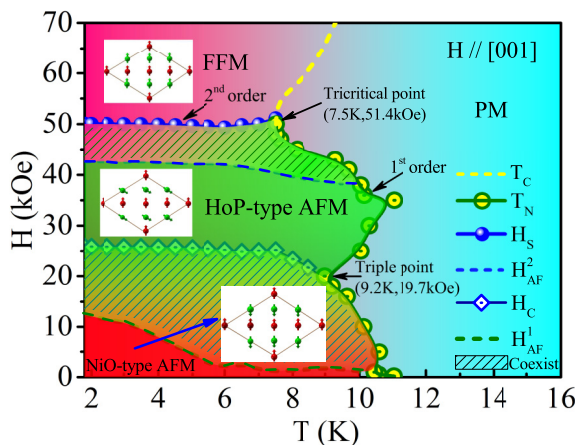


FIG. 4. H - T phase diagram around the phase transition temperature for single-crystal DySb with $H \parallel [001]$ (PM, AFM, and FFM represent paramagnetic, antiferromagnetic, and forced ferromagnetic phases, respectively).

of AFM phases coexist in a large range from ~ 10 kOe to ~ 25 kOe. In the field range of ~ 25 kOe to ~ 42 kOe, DySb enters a single phase of HoP-type AFM, as depicted in the middle inset of Fig. 4. Upon further increasing the field, the HoP-type AFM is polarized gradually into a FFM state, where the HoP-type AFM and the FFM phases coexist from ~ 42 kOe to ~ 50 kOe. The FFM state finally dominates the phase diagram when the field exceeds 50 kOe. Due to the multiple field-induced phases, DySb exhibits a field-induced tricritical mean-field behavior. Usually, a tricritical point is used to describe the intersection of three critical lines [6]. For DySb, three phases (i.e., HoP-type AFM, FFM, and PM) join at such a tricritical point, which is located at the field and temperature of (7.5 K, 51.4 kOe). In addition, a triple point is also found at (9.2 K, 19.7 kOe), which is located at the intersection point of NiO-type AFM, HoP-type AFM, and PM phases. It is well known that the phase transition from PM to AFM is of a first-order type, accompanied with a structural transition from cubic to tetragonal. The tricritical point is exactly at the terminal of this first-order phase transition boundary, which is located at the point among three absolutely different phases. Differently, the triple point is at the terminal of boundaries between two AFM states, which still belongs to the first-order transition. This triple point is also different from a Lifshitz point which is a special multicritical one with an incommensurate phase joining all three phases with a common tangent [33]. The multiple field-induced phase has also been reported for $H \parallel [110]$, in which the tricritical point located at (8.5 K, 14.7 kOe) and the triple point at (9.7 K, 12.4 kOe) [17]. However, only one kind of AFM phase exists for $H \parallel [110]$. The various and coexisting phases in DySb indicate the delicate competition and balance of magnetic interactions in this system.

Recent studies have shown that the magnetic structure and magnetic interaction are essential to the formation and evolution of various topological nontrivial states. Usually, magnetic correlation and spin-orbital coupling play important roles in these processes. For instance, the occurrence of band inversion in CeBi strongly depends on the strength of spin-orbital coupling which determines the splitting of the p orbital and hybridization with the Ce t_{2g} orbital [36]. A similar phenomenon has been observed in DySb [13]. Theoretical calculations and transport experiments also

suggest a close relation between magnetic structures and band structures [12,37]. It has been proposed that the AFM ground state of NdSb is a Dirac semimetal state while the FFM state becomes a Weyl semimetal state with twofold degenerate crossing points. For DySb, theoretical calculations also predict the existence of a magnetic semimetal state in its FFM phase. However, the topological property in the two AFM phases still remains elusive. Particular efforts can be devoted to the tricritical point and triple point, each of which connects three distinct magnetic phases and is expected to cause a novel topological transition and special critical phenomenon. The investigations in the present work thus provide crucial information from the aspect of magnetic coupling and magnetic criticality.

IV. CONCLUSIONS

In summary, multiple field-induced phase transitions in DySb are investigated from aspects of critical analysis and phase diagram. As the field increases, two magnetic phase transitions are induced for $H \parallel [001]$, namely, from the NiO-type AFM ground state to the HoP-type AFM, and finally to the FFM phase. The study of critical behaviors gives critical exponents $\beta = 0.244(2)$, $\gamma = 0.827(2)$, and $\delta = 4.425(1)$ for $H \parallel [001]$, which are examined by the Widom law and scaling

equations. The deduced critical exponents are close to a tricritical mean-field model, suggesting a field-induced tricritical phenomenon. A detailed H - T phase diagram around the phase transition temperature for $H \parallel [001]$ is constructed, in which a field-induced tricritical point is revealed at the temperature and field of (7.5 K, 51.4 kOe), located at the intersection of the AFM, FFM, and PM phases. Moreover, a triple point is found at (9.2 K, 19.7 kOe), which is located among the NiO-type AFM, HoP-type AFM, and FFM phases. Such fascinating multiple field-induced phases and criticality are indicative of the delicate competition and balance in this system, and lays a solid foundation for future research in topological transition.

ACKNOWLEDGMENTS

This work was supported by the National Key R&D Program of China (Grant No. 2017YFA0303201), the National Natural Science Foundation of China (Grants No. 12074386, No. 11874358, No. 11574322, No. U1732276, No. 11974181, No. 11874363, and No. U1932216), the Users with Excellence Program of Hefei Science Center CAS (2019HSC-UE010), and the open research program from Science and Technology Commission of Shanghai Municipality (Grant No. 19DZ2270200). A proportion of this work was supported by the High Magnetic Field Laboratory of Anhui Province.

-
- [1] W. Metz, *Science* **181**, 147 (1973).
- [2] P. M. A. Mestrom, V. E. Colussi, T. Secker, G. P. Groeneveld, and S. J. J. M. F. Kokkelmans, *Phys. Rev. Lett.* **124**, 143401 (2020).
- [3] S. Yin, S.-K. Jian, and H. Yao, *Phys. Rev. Lett.* **120**, 215702 (2018).
- [4] M. Fisher, *Rev. Mod. Phys.* **46**, 597 (1974).
- [5] H. Stanley, *Introduction to Phase Transitions and Critical Phenomena* (Oxford University Press, London, 1971).
- [6] R. Griffiths, *Phys. Rev. Lett.* **24**, 715 (1970).
- [7] V. Taufour, D. Aoki, G. Knebel, and J. Flouquet, *Phys. Rev. Lett.* **105**, 217201 (2010).
- [8] F. Tafti, Q. Gibson, S. Kushwaha, N. Haldolaarachchige, and R. Cava, *Nat. Phys.* **12**, 272 (2016).
- [9] L.-K. Zeng, R. Lou, D. S. Wu, Q. N. Xu, P. J. Guo, L. Y. Kong, Y. G. Zhong, J. Z. Ma, B. B. Fu, P. Richard *et al.*, *Phys. Rev. Lett.* **117**, 127204 (2016).
- [10] J. Xu, F. Wu, J. Bao, F. Han, Z. Xiao, I. Martin, Y. Lyu, Y. Wang, D. Chung, M. Li *et al.*, *Nat. Commun.* **10**, 2875 (2019).
- [11] S. Jang, R. Kealhofer, C. John, S. Doyle, J. Hong, J. Shim, Q. Si, O. Erten, J. Denlinger, and J. Analytis, *Sci. Adv.* **5**, eaat7158 (2019).
- [12] Y. Wang, J. H. Yu, Y. Q. Wang, C. Y. Xi, L. S. Ling, S. L. Zhang, J. R. Wang, Y. M. Xiong, T. Han, H. Han *et al.*, *Phys. Rev. B* **97**, 115133 (2018).
- [13] D. Liang, Y. Wang, C. Xi, W. Zhen, J. Yang, L. Pi, W. Zhu, and C. Zhang, *APL Mater.* **6**, 086105 (2018).
- [14] Y. Wu, Y. Lee, T. Kong, D. Mou, R. Jiang, L. Huang, S. L. Bud'ko, P. C. Canfield, and A. Kaminski, *Phys. Rev. B* **96**, 035134 (2017).
- [15] W. Hu, J. Du, B. Li, Q. Zhang, and Z. Zhang, *Appl. Phys. Lett.* **92**, 192505 (2008).
- [16] E. Bucher, R. Birgeneau, J. Maita, G. Felcher, and T. Brun, *Phys. Rev. Lett.* **28**, 746 (1972).
- [17] P. Streit, G. Everett, and A. Lawson, *Phys. Lett. A* **50**, 199 (1974).
- [18] See Supplemental Material at <http://link.aps.org/supplemental/10.1103/PhysRevB.102.174417> for the crystal structure, XRD pattern of the single crystal, $M(T)$ and $M(H)$ curves at different temperature and field, and MAPs for different models.
- [19] W. Ban, D. Wu, B. Xu, J. Luo, and H. Xiao, *J. Phys.: Condens. Matter* **31**, 405701 (2019).
- [20] D. Li, S. Nimori, and T. Shikama, *Solid State Commun.* **150**, 1865 (2010).
- [21] A. Arrott and J. Noakes, *Phys. Rev. Lett.* **19**, 786 (1967).
- [22] K. Huang, *Statistical Mechanics*, 2nd ed. (Wiley, New York, 1987).
- [23] S. Kaul, *J. Magn. Magn. Mater.* **53**, 5 (1985).
- [24] J. Fan, L. Ling, B. Hong, L. Zhang, L. Pi, and Y. Zhang, *Phys. Rev. B* **81**, 144426 (2010).
- [25] L. Kadanoff, *Physics* **2**, 263 (1966).
- [26] B. Widom, *J. Chem. Phys.* **43**, 3898 (1965).
- [27] M. Otero-Leal, F. Rivadulla, S. S. Saxena, K. Ahilan, and J. Rivas, *Phys. Rev. B* **79**, 060401(R) (2009).
- [28] L. Zhang, D. Menzel, C. Jin, H. Du, M. Ge, C. Zhang, L. Pi, M. Tian, and Y. Zhang, *Phys. Rev. B* **91**, 024403 (2015).
- [29] A. K. Mishra and V. Ganesan, *Phys. Rev. B* **100**, 125113 (2019).

- [30] T. Sakakibara, S. Nakamura, S. Kittaka, M. Kakihana, M. Hedo, T. Nakama, and Y. Onuki, *J. Phys. Soc. Jpn.* **88**, 093701 (2019).
- [31] H. Han, W. Liu, Y. Dai, Y. Gao, Z. Tian, J. Fan, S. Zhou, L. Pi, C. Zhang, L. Zhang, and Y. Zhang, *Phys. Rev. B* **98**, 054403 (2018).
- [32] R. L. Stillwell, I.-L. Liu, N. Harrison, M. Jaime, J. R. Jeffries, and N. P. Butch, *Phys. Rev. B* **95**, 014414 (2017).
- [33] H. C. Chauhan, B. Kumar, J. K. Tiwari, and S. Ghosh, *Phys. Rev. B* **100**, 165143 (2019).
- [34] H. Han, L. Zhang, D. Sapkota, N. Hao, L. Ling, H. Du, L. Pi, C. Zhang, D. G. Mandrus, and Y. Zhang, *Phys. Rev. B* **96**, 094439 (2017).
- [35] G. Felcher, T. Brum, R. Gambino, and M. Kuznietz, *Phys. Rev. B* **8**, 260 (1973).
- [36] K. Kuroda, M. Ochi, H. S. Suzuki, M. Hirayama, M. Nakayama, R. Noguchi, C. Bareille, S. Akebi, S. Kunisada, T. Muro *et al.*, *Phys. Rev. Lett.* **120**, 086402 (2018).
- [37] L. Ye, T. Suzuki, C. R. Wicker, and J. G. Checkelsky, *Phys. Rev. B* **97**, 081108(R) (2018).